Electronic Band Structure Modeling in Strained Si-Nanowires: Two Band $\mathbf{k}\cdot\mathbf{p}$ Versus Tight Binding

Z. Stanojević, O. Baumgartner, V. Sverdlov, and H. Kosina
Institute for Microelectronics, Vienna University of Technology,
Gußhausstraße 27-29, Vienna, Austria
e-mail: (stanojevic|baumgartner|sverdlov|kosina)@iue.tuwien.ac.at

***Abstract*—The subband structure of silicon nanowires has gained much interest recently. Nanowires with diameters below 10 nm are predicted to have a significantly altered subband structure compared with bulk silicon. The effective mass approximation fails to describe these alterings correctly, and so far the semiempirical tight binding method and first principles calculations were used to investigate them. In this paper we present an approach based on a two band $\mathbf{k}\cdot\mathbf{p}$ description of the conduction band minima. The method excels in simplicity of modeling and versatility including the ability to model strain effects on the subband structure.**

I. Introduction

Nanostructures such as nanowires exhibit band structure effects that cannot be captured by the single band effective mass approximation. For very thin structures these effects include nonparabolicity, change of effective mass in axial direction and subband splitting. All these effects have already been investigated using the semiempirical tight binding approach [4, 7], first principles calculations [6] and by applying nonparabolicity corrections to the effective mass approximation [2]. In this work we rely on a different method: A two band $\mathbf{k}\cdot\mathbf{p}$ Hamiltonian is used to model the electronic band structure. The Hamiltonian contains only one additional parameter in the coupling term while the other terms are derived from the effective mass approximation. It also includes deformation potentials for both uniaxial and shear strain. As we shall see, these few parameters are sufficient to obtain an accurate picture of the subband structure within the transport-relevant energy range.

II. Model

The model Hamiltonian used here was introduced by Hensel et al. [1] to describe the electronic band structure behavior in strained bulk silicon. The Hamiltonian is derived from $\mathbf{k}\cdot\mathbf{p}$ theory by expanding the electronic band structure around one of the X points. The description involves two Δ valleys adjacent to the X point, the remaining bands are treated as perturbation. Contrary to the common six and eight band $\mathbf{k}\cdot\mathbf{p}$ models which use an expansion around the Γ point, the two bands in our model touch at the X point. The Hamiltonian reads as follows:

$$\begin{aligned}\mathbf{H} = &\left(\frac{\hbar^2(k_{\mathrm{t}1}^2+k_{\mathrm{t}2}^2)}{2m_{\mathrm{t}}}+\frac{\hbar^2 k_{\mathrm{l}}^2}{2m_{\mathrm{l}}}+\Xi_{\mathrm{u}}\varepsilon_{\mathrm{l\text{-}l}}+V\right)\mathbf{I}\\ &+\frac{\hbar^2 k_0 k_{\mathrm{l}}}{m_{\mathrm{l}}}\,\boldsymbol{\sigma}_x-\left(\frac{\hbar^2 k_{\mathrm{t}1}k_{\mathrm{t}2}}{M}-2\Xi_{\mathrm{u}'}\varepsilon_{\mathrm{t1\text{-}t2}}\right)\boldsymbol{\sigma}_z.\end{aligned} \tag{1}$$

V denotes the conduction band edge; $m_{\mathrm{l}}=0.91m_e$ and $m_{\mathrm{t}}=0.19m_e$ are the known longitudinal and transversal effective masses of silicon; $k_0=0.15\frac{2\pi}{a}$ amounts to the distance between the X and the adjacent band minima; $\varepsilon_{\mathrm{l\text{-}l}}$ and $\varepsilon_{\mathrm{t1\text{-}t2}}$ are the respective uniaxial and shear strain components in the valley coordinate system, $(\mathrm{l},\mathrm{t}1,\mathrm{t}2)$, and Ξ_{u}=9.0 eV and $\Xi_{\mathrm{u}'}$=7.0 eV the corresponding deformation potentials; $\boldsymbol{\sigma}_{x,z}$ denote the Pauli matrices and $\mathbf{I}$ the identity matrix.

$$\mathbf{I}=\begin{pmatrix}1&0\\0&1\end{pmatrix},\boldsymbol{\sigma}_x=\begin{pmatrix}0&1\\1&0\end{pmatrix},\boldsymbol{\sigma}_z=\begin{pmatrix}1&0\\0&-1\end{pmatrix}. \tag{2}$$

The band coupling "mass" M is determined by the interband matrix elements. In [1] the authors of the model gave an approximate value for it,

$$\frac{1}{M}\approx\frac{1}{m_{\mathrm{t}}}-\frac{1}{m_e}, \tag{3}$$

which was recently confirmed by EPM results [5].

The model was found to give an accurate description of the bulk band structure in an area of $0.25(2\pi/a)$ around k_0 and up to 0.5 eV above the conduction band minimum [5]. We assume that the accuracy also holds for subbands within this energy range.

In (1) we used a $(\mathrm{l},\mathrm{t}1,\mathrm{t}2)$ coordinate system, which is aligned to the (100), (010), and (001) crystallographic axes as shown in Fig. 1. To cover all conduction band valleys in silicon, the Hamiltonian must be solved for three different orientations. Thus, it is rotated three times according to the growth direction of the nanowire and its face orientations and quantized in the cross section plane. The quantization is achieved by replacing $\mathbf{k}$ with $[-i\partial_x\ -i\partial_y\ k_{\|}]$, which gives an expression for (1) containing all sorts of first and second order derivative terms since in the general case the crystal and device coordinate system are not aligned. The resulting differential equation is discretized using box integration and solved for each $k_{\|}$-value using efficient numerical algorithms available through the Vienna Schrödinger Poisson framework (VSP) [3].

III. Simulation and parameter extraction

We studied square and circular shaped nanowires of varying diameters. Different stresses along the nanowire axis were also applied. The behavior of the subband structure with respect to confinement and stress was of primary interest here.

978-1-4244-9382-1/10/$26.00 ©2010 IEEE

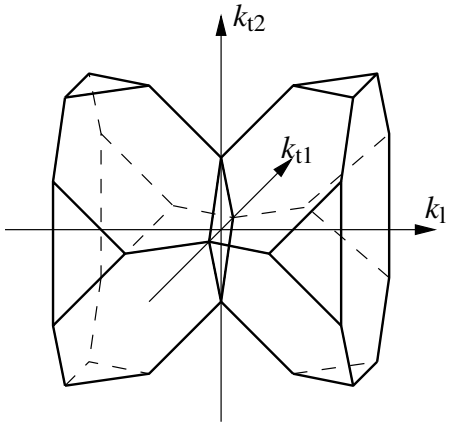

Fig. 1. The coordinate system of the Hamiltonian at one of the X points

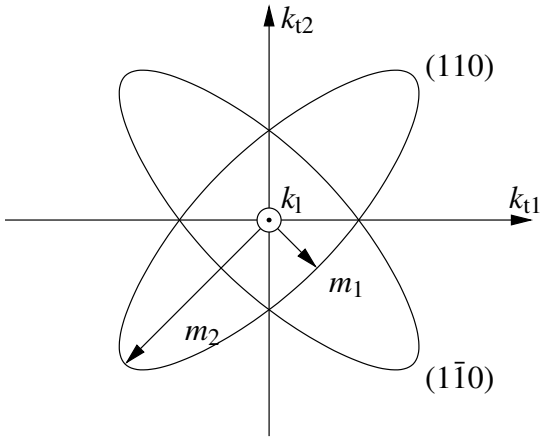

Fig. 2. Cut through the bulk band structure at the X point showing two different effective masses for the [110] directions

The change of the effective mass was taken as an quantity representrative of the subband structure alterations due to confinement and stress.

To obtain a singular, meaningful value for the effective mass one cannot simply use the curvature of the lowest subband, since thicker nanowires tend to have subbands that are closely spaced energetically (less than $k_B T$) and thus not only influence each other but also show different curvatures at their respective minima. This is especially the case for [110] oriented nanowires because the bulk band structure has two different curvatures when viewed along a [110] axis, as sketched in Fig. 2. As thickness increases the effective mass of the lowest subbands become more and more indeterminate.

To mitigate these problems a different approach is chosen here. When subjected to a small field the electron ensemble will respond with a average effective mass. Assuming that that the electron ensemble in the nanowire has the properties of an ideal one dimensional gas, i.e. Boltzmann statistics and only minor nonparabolicity, the average effective mass can be derived from the relation

$$\frac{1}{2} m^*_{\text{avg}} \left\langle v_g^2 \right\rangle = \frac{1}{2} k_B T, \tag{4}$$

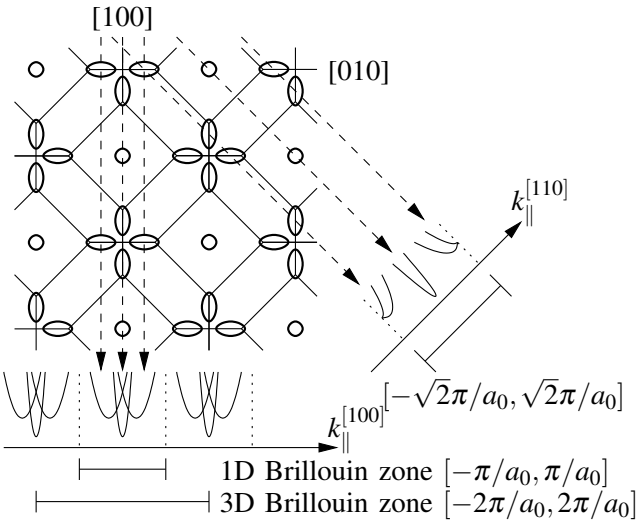

Fig. 3. Schematic picture of the projection of the bulk valleys onto the one dimensional k-space through confinement

where v_g is the group velocity which can be readily obtained from the subband structure. The 1/2-factor on the right hand side is due to the electron gas having only one degree of freedom in the nanowire.

IV. Results and discussion

Nanowires of [100], [110] and [111] growth orientation of both circular and square cross sections have been simulated. The subband structure for a circular 5 nm thick nanowire is shown in Fig. 4. In the case of the [100] nanowire confinement causes the minima of the unprimed subbands to be projected onto $k_{\parallel} = 0$, i.e. the Γ point of the one dimensional Brillouin zone, and the minima of the primed subbands at $k_{\parallel} = \pm k_0$ (see Fig. 3). While unprimed subbands of the [100] nanowire are four-fold degenerate, the degeneracy is lifted for the [110] nanowire. This is due to the ambiguous confinement effective mass in $(1\bar{1}0)$ direction as discussed in Fig. 2. Fig. 5 illustrates the degeneracy lifting. For the [111] nanowire the subband minima are not projected onto the Γ point. Instead, the subbands split at the Γ point.

The axial effective mass versus nanowire thickness is shown in Fig. 7 and 8. It shows that the effective mass deviates strongly from the bulk limit for very thin nanowires. While the effective mass increases for [100] and [111] nanowires, it decreases for [110] nanowires. This will be of importance for future nanowire based devices. In Fig. 8 the effective mass dependence displays a non-monotonous behavior. The inset in the figure shows why: Confinement opens a gap between the first and second subband at the Γ point. Eventually, the two separate valleys merge into one passing the point where the lowest subband forms a fourth order flat at its bottom, giving a sharp effective mass peak.

In order to verify our model data generated by 10-band $sp^3d^5s^*$ semiempirical tight binding simulations [4, 7] is also shown in Fig. 7. The agreement between the methods is reasonably good. Although the figure gives the impression

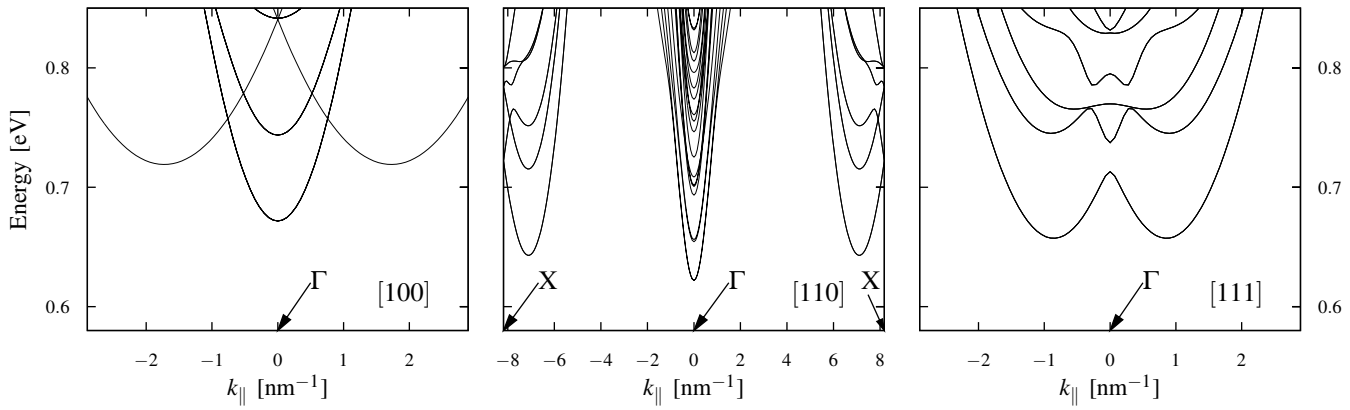

Fig. 4. Subband structure of circular 5 nm thick nanowires with [100], [110] and [111] growth orientations

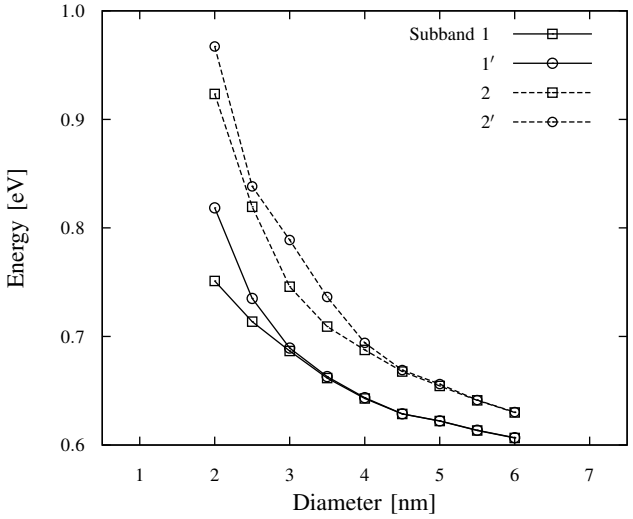

Fig. 5. Subband minima over (circular [110]) nanowire thickness. For low diameters the subband structure exhibits splitting effects

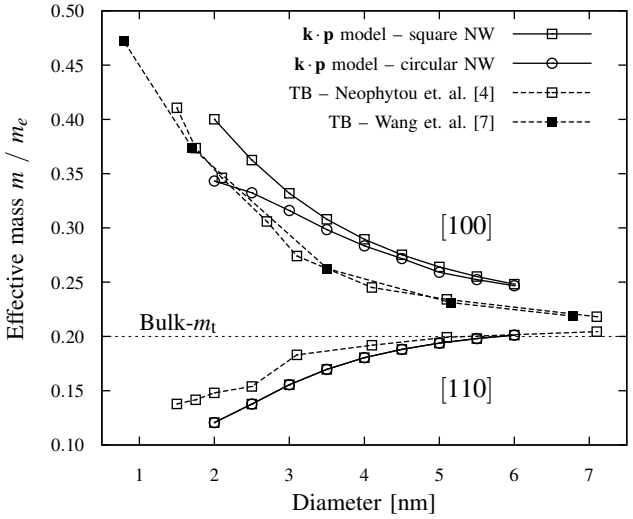

Fig. 7. Effective masses vs. thickness for [100] and [110] orientations showing good agreement with tight binding data

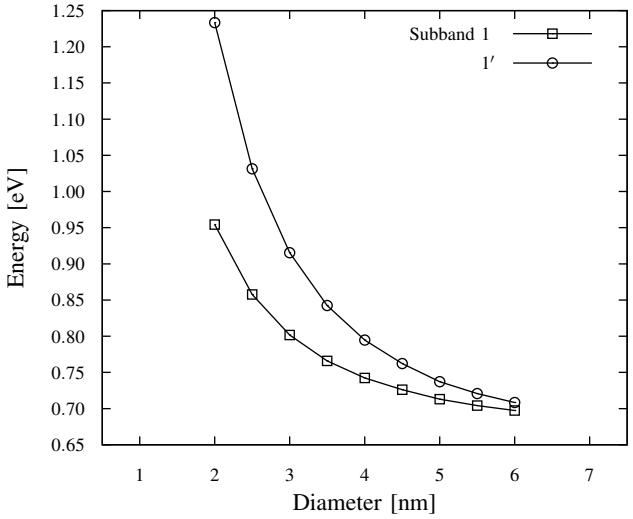

Fig. 6. Subband energy of circular [111] nanowires at the Γ point over thickness

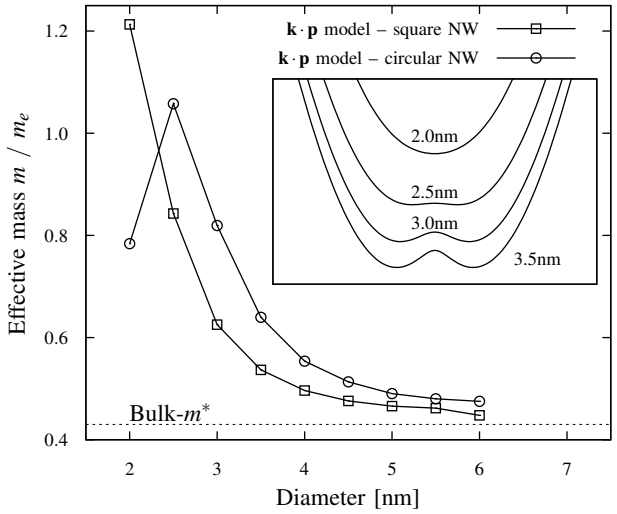

Fig. 8. Effective mass vs. thickness for [111] growth orientation; inset shows the lowest subband for round nanowires

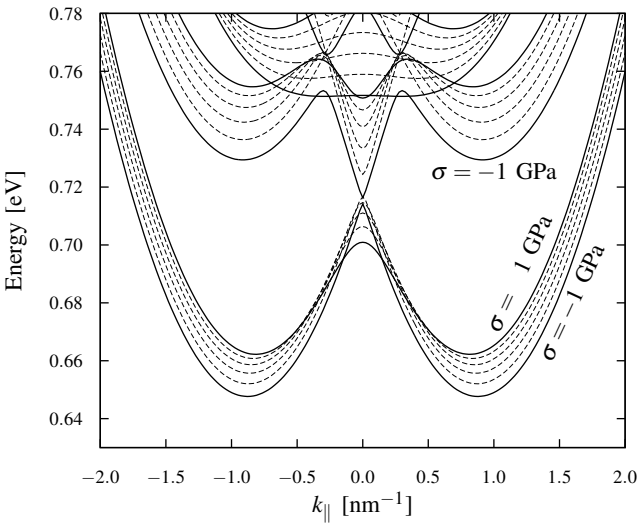

Fig. 9. Subband of a 5 nm [111] wire with varying axial stress showing subband splitting at the Γ point

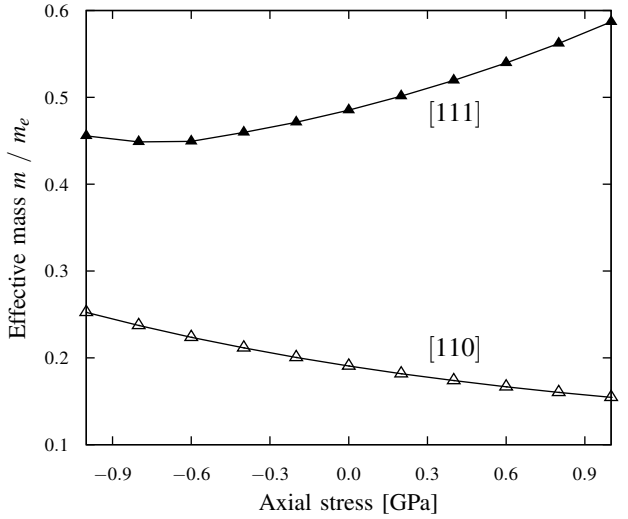

Fig. 10. Stress dependence of the effective mass of 5 nm thick [110] and [111] wires at the Γ point

that the [100] curve does not approach the bulk value of the effective mass, a power-law can be fitted to the points giving a curve that approaches the bulk effective mass at $\Delta m^*/m_0 = (d/d_0)^{-3/4}$.

Stressing the nanowire along its axis produces effects similar to confinement. Tensile stress applied to the [111] nanowire increases the splitting of the subbands at the Γ point while compressive stress has the opposite effect (Fig. 9). Also the effective mass is affected by stress in the same way it is affected by confinement: the effective mass decreases in [110] and increases in [111] nanowires when tensile stress is applied (Fig. 10). Stressing [100] nanowires produces merely an energy shift of the primed subbands, which is not shown here.

V. Summary and Conclusions

We have presented an alternative method for the calculation of nanowire subband structures based on a two band $\mathbf{k}\cdot\mathbf{p}$ model. The model introduces only one additional parameter, M, with respect to the effective mass approximation in contrast to the $sp^3d^5s^*$ model which needs ten parameters to be fitted to measurements. Our model gives good results even for nanowires of a few nanometers in diameter. Including two deformation potentials in the model allows the study of strain effects on the subband structure.

The results show a strong dependence of the subband structure on confinement and strain. We observed that the effective mass along the nanowire axis can be engineered, by controlling geometry and applying stress. For [110] nanowires the effective mass can even be reduced. These considerations need to be taken into account in the design of future devices and applications based on thin silicon nanowires.

Acknowledgment

This work has been supported by the Austrian Science Fund, special research program F2509.

References

[1] J. C. Hensel, H. Hasegawa, and M. Nakayama, "Cyclotron Resonance in Uniaxially Stressed Silicon. II. Nature of the Covalent Bond," *Phys. Rev.*, vol. 138, no. 1A, pp. A225–A238, Apr 1965.

[2] S. Jin, M. V. Fischetti, and T.-w. Tang, "Theoretical Study of Carrier Transport in Silicon Nanowire Transistors Based on the Multisubband Boltzmann Transport Equation," *Electron Devices, IEEE Transactions on*, vol. 55, no. 11, pp. 2886 –2897, nov. 2008.

[3] M. Karner, A. Gehring, S. Holzer, M. Pourfath, M. Wagner, W. Goes, M. Vasicek, O. Baumgartner, C. Kernstock, K. Schnass, G. Zeiler, T. Grasser, H. Kosina, and S. Selberherr, "A multi-purpose Schrödinger-Poisson Solver for TCAD applications," *Journal of Computational Electronics*, vol. 6, no. 1, pp. 179–182, Sep. 2007.

[4] N. Neophytou, A. Paul, M. Lundstrom, and G. Klimeck, "Bandstructure Effects in Silicon Nanowire Electron Transport," *Electron Devices, IEEE Transactions on*, vol. 55, no. 6, pp. 1286 –1297, june 2008.

[5] V. Sverdlov, G. Karlowatz, S. Dhar, H. Kosina, and S. Selberherr, "Two-band $\mathbf{k}\cdot\mathbf{p}$ model for the conduction band in silicon: Impact of strain and confinement on band structure and mobility," *Solid-State Electronics*, vol. 52, no. 10, pp. 1563–1568, 2008.

[6] H. Tsuchiya, H. Ando, S. Sawamoto, T. Maegawa, T. Hara, H. Yao, and M. Ogawa, "Comparisons of Performance Potentials of Silicon Nanowire and Graphene Nanoribbon MOSFETs Considering First-Principles Bandstructure Effects," *Electron Devices, IEEE Transactions on*, vol. 57, no. 2, pp. 406 –414, feb. 2010.

[7] J. Wang, A. Rahman, A. Ghosh, G. Klimeck, and M. Lundstrom, "On the validity of the parabolic effective-mass approximation for the I-V calculation of silicon nanowire transistors," *Electron Devices, IEEE Transactions on*, vol. 52, no. 7, pp. 1589–1595, July 2005.